Renormalization-group treatment of a Potts lattice gas for krypton adsorbed onto graphite

A. N. Berker and S. Ostlund
Department of Physics, Harvard University, Cambridge, Massachusetts 02138

F. A. Putnam
Department of Chemical Engineering, Massachusetts Institute of Technology, Cambridge, Massachusetts 02139
(Received 31 October 1977)

Krypton atoms adsorbed in submonolayer quantities onto the basal graphite surface may be represented by a triangular lattice gas with nearest-neighbor exclusion and further-neighbor attraction decreasing with separation. We view this as a three-state Potts model with thermodynamic vacancies which are controlled by a chemical potential. A position-space renormalization-group treatment is performed by adapting Migdal's approximate recursion to the triangular lattice, and results are compared with experimental data. Our temperature versus density phase diagram for krypton submonolayers has an in-registry solid phase separated from a liquid phase by a line of continuous (Potts tricritical) transitions at higher temperatures. At lower temperatures, the solid phase is separated from a gas phase by first-order transitions. The Potts tricritical line meets the coexistence region of the first-order transitions at an isolated fourth-order transition point. This point may be related to the transition of the triplet Ising model, solved exactly by Baxter and Wu. Our "Potts lattice gas" global phase diagram is in a three-parameter space of pair-interaction constants and chemical potential. It contains solid, liquid, and gas phases, variously separated by first-order, Ising critical, three- and four-state Potts, and fourth-order transitions. The Lennard-Jones potential between krypton adatoms determines the planar subspace applicable to krypton submonolayers. Other planes, similarly determined, are applicable to adsorbed nitrogen, methane, and ethane, for which we estimate the temperatures of the fourth-order points. Our treatment also predicts a tricritical end-point topology, instead of the fourth-order point topology, when second-neighbor adatom pair attraction is not much stronger than third- and fourth-neighbor attractions.

I. INTRODUCTION

Physisorbed films[1] have in recent years provided experimental realizations of two-dimensional phase transitions.[2] Graphite is extensively used[3-12] as a substrate. Its hexagonal basal plane presents a regular array of preferred adsorption sites, namely the hexagon centers. These adsorption sites form a triangular lattice [Fig. 1(a)]. Adsorbed atoms are taken to interact pairwise: For commonly studied adsorbates,[3-12] two atoms experience a positive (unfavorable) potential when adsorbed onto nearest-neighbor sites, and a negative potential increasing to zero with separation

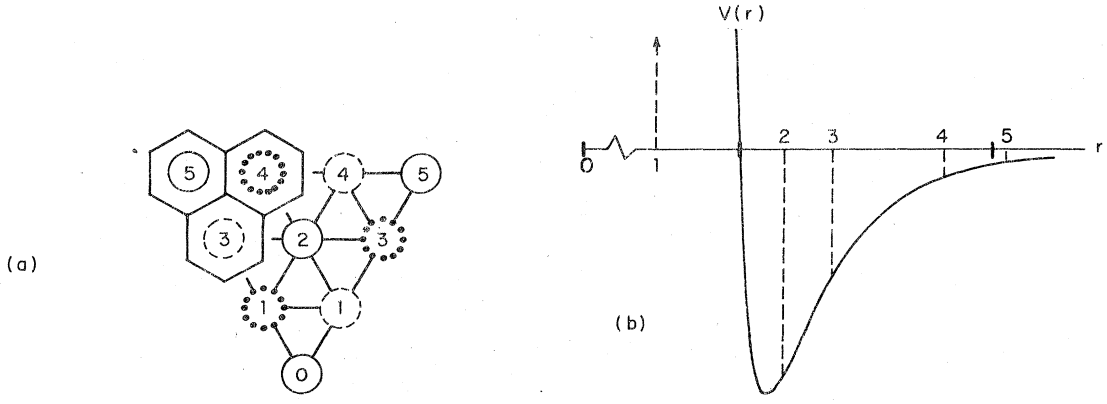

FIG. 1. (a) Adsorption sites of the basal plane of graphite: They occur at the centers of the graphite hexagons, three of which are displayed. These adsorption sites form a triangular lattice which is composed of three sublattices, distinguished here by full, dashed, and dotted circles. At krypton monolayer completion, all sites of one sublattice are occupied, and the other two sublattices have all their sites empty. Numbers indicate first- through fifth-neighbors of the site labeled 0. (b) Lennard-Jones potential $V(r)$ between two krypton atoms adsorbed onto graphite [Eq. (2.1)]. The well depth is $\epsilon = k \times (145\,^{\circ}\mathrm{K})$, and $V(r)$ changes sign at the LJ diameter $\sigma = 3.60$ Å (Ref. 8). Numbers indicate first- through fifth-neighbor separations on the adsorption-site lattice.

when adsorbed onto further-neighbor sites [Fig. 1(b)]. Two-dimensional phase transitions have been observed in submonolayers of helium,[3,4] neon,[5] krypton,[6-9] xenon,[6] nitrogen,[10-12] and methane[6] adsorbed onto graphite. An "in-registry solid" phase, whose crystalline structure consists of a preferential occupation of one of the three sublattices in the adsorption-site lattice, has been distinguished from "disordered fluid" phases with, on the average, equivalent occupation of each sublattice. It seems reasonable to develop a theory for these transitions through a two-dimensional lattice-gas model.[13] Exact results for such models are known at isolated special cases of equivalence to the two-dimensional spin-$\frac{1}{2}$ Ising model[14] with nearest-neighbor interaction only and zero magnetic field, but no exact solution has been achieved over the continuous range of experimental applicability. The Bethe-Peierls approximation has been applied[15] to such a model for helium adsorbed onto graphite, resulting in first-order phase transitions, in disagreement with experiment.[3,4] This can be associated with the failure of mean-field-type approximations, which do not yield the known continuous transition[16,17] of the two-dimensional three-state Potts model,[18] since the helium monolayer transition has been argued[19] to belong to the universality class of this Potts transition. More recently, Schick, Walker, and Wortis[20] have achieved excellent agreement with experiment[3,4] by performing the position-space[21,22] renormalization-group[23] treatment of a helium lattice-gas model.

Krypton submonolayers adsorbed onto the graphite basal plane are of particular interest because vapor-pressure experiments[6-8] have produced a *multicritical* phase diagram (Fig. 2). The solid and fluid phases mentioned above are separated by a line of continuous phase transitions[6,8] at the higher temperatures; at lower temperatures, the two phases are separated by first-order phase transitions.[6,7] It has been inferred[8] that the line of continuous transitions meets the coexistence region of the first-order transitions at an isolated higher-order transition point in the temperature-density phase diagram.

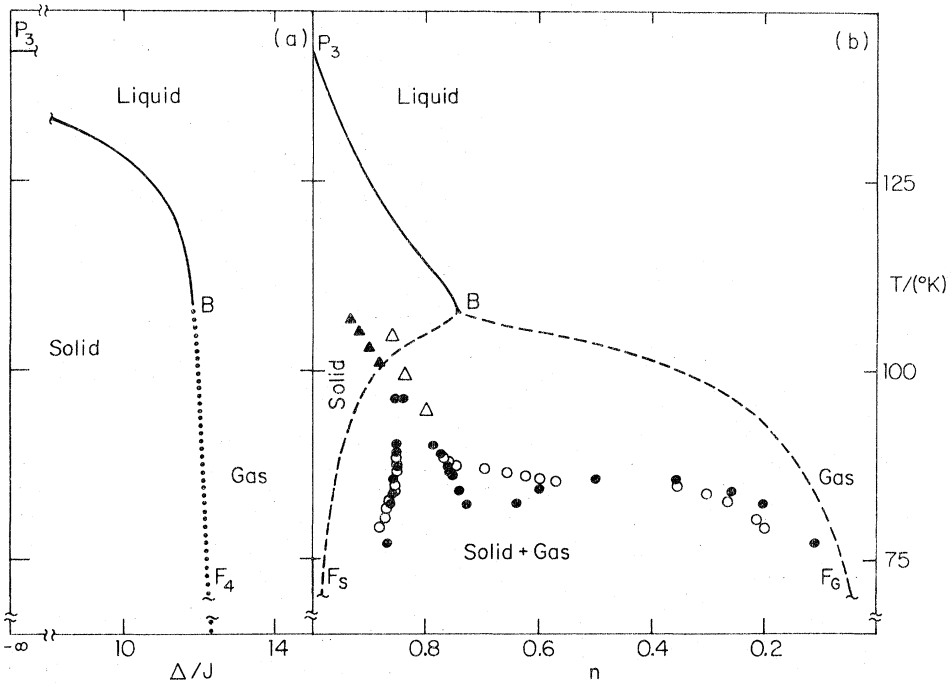

FIG. 2. Phase diagrams for krypton submonolayers (Sec. II B) resulting from our PLG treatment: In the temperature vs. chemical potential diagram (a), F_4B (dotted) is a line of first-order transitions; F_SBF_G (dashed) is the corresponding phase-separation boundary in the temperature vs. density diagram (b). In both (a) and (b), P_3B is a line of Potts tricritical transitions, and B is a fourth-order point. In the temperature vs. density diagram, the following points from vapor-pressure experiments are shown: first-order transitions from Ref. 6 (●) and Ref. 7 (○); higher-order transitions from Ref. 6 (▲) and Ref. 8 (△). The density values for Ref. 8 are obtained using the graphite surface area of 11.8 m^2/g determined from compressibility minima. Densities in Ref. 6 are given as θ, fractions of the close-packed monolayer coverage; multiplication by 1.098 converts these to n, fractions of the in-registry monolayer coverage. The density scale of Ref. 7 is determined by adjusting the high-density points to Ref. 6.

In this research, we study submonolayers of medium-sized atoms or molecules (larger than neon, smaller than xenon) adsorbed onto the graphite basal plane. Although we start our treatment from a microscopic picture of adsorbed krypton, it will be seen that our model is applicable to a number of adsorbates, such as nitrogen, methane, and ethane. We obtain a global multicritical phase diagram[24] in the space of three thermodynamic fields, and the subspace applicable to a given adsorbate is determined by the corresponding adatom size. Thus, phase transitions of different types of submonolayers are unified into one global diagram characterized by a few distinct sets of critical exponents, in agreement with the universality hypothesis.[25]

We obtain the line of continuous phase transitions of krypton submonolayers as a line of three-state Potts tricritical points,[16-18,24] like the helium case.[19] The isolated point terminating this line is a fourth-order transition point which may be related to the (fourth-order) transition of the triplet Ising model.[26] The eigenvalues from our approximate renormalization-group analysis agree to 1% with Baxter and Wu's exact solution[26] of the latter transition. However, there are symmetry and eigendirection differences between these two transitions. In our temperature versus density phase diagram, the two branches of the phase-separation line form a cusp as the first-order coexistence region reaches this fourth-order point from the low-temperature side (Fig. 2).

Our method consists of two distinct parts. First, we further develop the lattice-gas modeling of submonolayers, by approximating the krypton lattice gas (KLG) by a "Potts lattice gas" (PLG): a three-state Potts model with thermodynamic[27] vacancies controlled by a chemical potential. This step, called a prefacing[28] transformation, relies on the *nearest-neighbor exclusion* (very large positive potential) in the KLG (Fig. 1). Each PLG site represents three KLG sites (Fig. 3). We are then able to take into account the KLG second-, third-, and fourth-neighbor negative potentials. These further-neighbor interactions destroy an infinite ground-state degeneracy at the zero-temperature transition, thus converting it from continuous to first-order and inducing a multicritical phase diagram. Second, we adapt Migdal's approximate recursion relation[29,30] to the triangular lattice and perform a global[24] position-space[21,22] renormalization-group[23] treatment of the PLG. It is of technical interest that exceedingly simple recursion relations [Eq. (2.9)] yield[31] a complex phase diagram (Fig. 6), resulting from thirteen separate fixed points[32] (Fig. 5): A space of three thermodynamic fields is portioned into solid, liquid, and gas phases. These three phases are separated by a surface of Potts tricritical points, and two surfaces of first-order transitions. These three surfaces are variously bounded by a line of fourth-order points, an Ising critical line, and a line of Potts tricritical end-points. These three lines meet at the transition point of the four-state Potts model.[18] A Potts tricritical end-point topology (Fig. 9) is predicted [instead of the fourth-order point topology (Fig. 2) described above for krypton] for hypothetical adsorbates with the second-neighbor potential not much more negative than the third- and fourth-neighbor potentials. However, all adsorbates to which we applied our model corresponded to the topology displayed in Fig. 2. Our treatment does not include second-layer adsorption[6,8] and behavior incommensurate[33] with the graphite substrate which occur around monolayer completion.

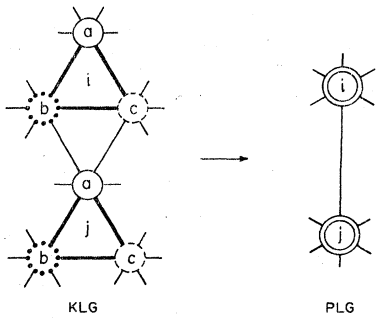

FIG. 3. Three nearest-neighbor sites of the krypton lattice gas (KLG) are represented by one site of the Potts lattice gas (PLG), as prescribed in Sec. II A. A given KLG site is in one of two states (empty or occupied), while a given PLG site is in one of four states (empty, occupied at a, b, or c). Both the KLG and PLG sites form, among themselves, triangular lattices, but the PLG lattice constant is $\sqrt{3}$ times the KLG one, and the two lattices are rotated by 30° with respect to each other.

In Sec. II, we construct the PLG model, obtain exact information by considering its special cases, and derive our recursion relations. In Sec. III, we describe the resulting global phase diagram for the PLG, then discuss and compare with experiment[6-8] our predicted krypton submonolayer phase diagram. We also estimate the temperatures of the fourth-order points for nitrogen, methane, and ethane.

II. METHOD

A. Potts lattice-gas model

The hexagonal basal plane of graphite presents a regular array of preferred adsorption sites,

namely the hexagon centers.[1] Each adsorption site can be either empty, or occupied by a single adatom. The adsorption sites form a triangular lattice [Fig. 1(a)], with a nearest-neighbor separation of 2.46 Å. Fig. 1(b) shows the Lennard-Jones (LJ) potential $V(r)$ between two graphite-adsorbed krypton atoms, deduced[8] from experimental adsorbate-adsorbent virial coefficients

$$V(r)=4\epsilon\left[\left(\frac{\sigma}{r}\right)^{12}-\left(\frac{\sigma}{r}\right)^{6}\right], \tag{2.1}$$

with LJ well depth $\epsilon = k\times(145\ ^\circ\mathrm{K})$, where k is the Boltzmann constant; $V(r)$ changes sign at the LJ diameter $\sigma = 3.60$ Å. The first- through fifth-neighbor separations are indicated by the numbers on the r axis. The very large (350 times the well depth) positive potential of a would-be nearest-neighbor pair causes *nearest-neighbor exclusion.* Further-neighbor interactions are favorable (negative potential) and essentially short ranged. Thus the krypton monolayer is completed when one of the three triangular sublattices [Fig. 1(a)] is entirely occupied, while the other two are empty. As the submonolayer approaches this state, assuming no formation of multilayer patches, one sublattice is preferentially occupied. This signifies a breaking of the translational symmetry of the *krypton lattice gas*, which will happen in one of three degenerate ways, distinguished by the one sublattice which has the larger share of adatoms.

In order to make the krypton submonolayer problem more amenable to renormalization-group treatment, we approximated, using the nearest-neighbor-exclusion property, the krypton lattice gas (KLG) described above by a *Potts lattice-gas* (PLG) model. Consider an elementary triangle, composed of three nearest-neighbor sites of the KLG, for example triangle i in Fig. 3. Taken as a whole, this triangle is in one of four states: It can contain no krypton adatom, or it can contain a single krypton adatom in position a, b, or c. We view such an elementary triangle as a single PLG site. Two variables (t_i, s_i) are assigned to it: t_i is 0 if the triangle is empty, 1 if it contains an adatom; in the latter case, a second variable $s_i = a$, b, or c describes the specific position of the adatom. A regular pattern of nonintersecting elementary triangles (two of which are shown in Fig. 3) completely covers the KLG. This pattern is itself a triangular lattice, so that the PLG sites form a triangular lattice, but with nearest-neighbor separation larger by a factor of $\sqrt{3}$ than that of the KLG lattice, and rotated by 30° from the KLG lattice. Although Fig. 3 is reminiscent of a renormalization-group (rescaling) transformation,[21] the step taken in this subsection is to be distinguished as a one-time prefacing (restructuring) transformation.[28]

TABLE I. Krypton pair potentials $-\beta V$, as assigned by our PLG model [Eq. (2.2)] and by the experimentally determined (Ref. 8) LJ potential [Eq. (2.1)]. T is temperature in degrees Kelvin.

Krypton pair type on KLG lattice	PLG	LJ
Second neighbors	$K+2J$	$134/T$
Third neighbors	$K-J$	$75/T$
Fourth neighbors	$K-J$	$16/T$
Fifth and further	0	$<8/T$

We studied the PLG with the Hamiltonian

$$-\beta\mathcal{H} = -\beta\sum_{\langle ij\rangle} V_{ij}t_it_j - \Delta\sum_i t_i\,, \tag{2.2a}$$

$$-\beta V_{ij} = J(3\delta_{s_is_j}-1)+K\,, \tag{2.2b}$$

where the first sum is over all nearest-neighbor pairs of PLG sites, the second sum is over all PLG sites, $\beta\equiv 1/kT$ has been absorbed into the interaction constants J, K, and Δ, and $\delta_{s_is_j}$ is 1 (0) for $s_i = s_j$ ($s_i \neq s_j$). According to (2.2a), adatoms have[34] a chemical potential $-\beta^{-1}\Delta$, and interact through a pair-potential V_{ij} when occupying nearest-neighbor PLG sites. The J term in (2.2b) is determined by whether or not the two adatoms of a pair are on the same KLG sublattice. The calculational advantage gained by (2.2) is that a PLG with only nearest-neighbor interactions does take into account further-neighbor interactions of the underlying KLG. This is illustrated in Table I, which gives the potentials assigned by (2.2) to an adatom pair at various separations on the KLG lattice. Their LJ counterparts (2.1) are also given, and from this table one sees that a reasonable match to the krypton submonolayer problem is achieved by setting

$$K+2J = 134/T\,, \tag{2.3a}$$

$$K-J = \tfrac{1}{3}(75/T)+\tfrac{2}{3}(16/T)\,. \tag{2.3b}$$

The weights in the averaging in (2.3b) are so chosen because, on a triangular lattice, there are twice as many fourth-neighbor pairs as third-neighbor pairs. This PLG only approximates the KLG, since the nearest-neighbor-exclusion property of the latter is obeyed within each PLG site, but not when two PLG sites are involved: For example, referring to Fig. 3, the simultaneous occupation of (ja) and (jb) is not allowed, but (ja) and (ib) can be simultaneously occupied, being assigned the potential in (2.3b). This approximate nature of our prefacing transformation can be systematically improved,[28] resulting in PLG models with more types of interaction. Nevertheless, as discussed above, the essential consequence of

KLG nearest-neighbor exclusion is the introduction of three degenerate ground states, which is captured by the PLG here: Whereas the second term in (2.2b) amounts to an ordinary lattice-gas interaction, the first term is a three-state Potts[18] interaction. Indeed, the model made precise by (2.2) can be viewed as a *three-state Potts model*, but *with vacancies* in the form of *thermodynamic impurities*.[27,35] The average concentration of vacancies is controlled by Δ. Finally, by applying Kadanoff's procedure,[22] it can be shown that the PLG free energy is a lower bound to the KLG free energy.

The PLG studied here is a special case, delimited by a threefold symmetry, of the spin-$\frac{3}{2}$ Ising model with generalized nearest-neighbor interactions. As a *three*-state Potts model with vacancies, it is also a direct adaptation of the extensively studied Blume-Emery-Griffiths model,[36,37] a *two*-state Potts model with vacancies.

B. Exact information from special cases

Although our interest is in krypton submonolayers (Sec. III B, C), we first have to study the global J, K, Δ space phase diagram (Sec. III A) of the PLG (2.2), because the subspace (2.3) applicable to the submonolayer problem is not closed under our renormalization-group transformation (Sec. II C). A global description does have the advantage of providing a unified understanding of the behaviors of various adsorbates (Sec. III D). In distinguishing different thermodynamic phases in the remainder of this work, the following densities will be mentioned:

$$n(J,K,\Delta) \equiv \langle t_i \rangle = Z^{-1} \sum_{\{(t,s)\}} t_i e^{-\beta \mathcal{H}}, \tag{2.4}$$

$$n_a(J,K,\Delta) \equiv \langle t_i \delta_{s_i a} \rangle = Z^{-1} \sum_{\{(t,s)\}} t_i \delta_{s_i a} e^{-\beta \mathcal{H}}, \tag{2.4a}$$

where the sums are over all (t,s) configurations, the translational invariance of (2.2) makes i arbitrary, and Z is the partition function

$$Z(J,K,\Delta) = \sum_{\{(t,s)\}} e^{-\beta \mathcal{H}}. \tag{2.5}$$

n is the overall density of adatoms, and n_a is the density of adatoms on KLG sublattice a. n_b and n_c are defined similarly to (2.4a), and $n = n_a + n_b + n_c$. Before launching a position-space renormalization-group treatment, it is useful[24] to catalog any available exact information on the phase diagram under study.

1. Ordinary lattice-gas plane. In the $J=0$ plane, $n_a = n_b = n_c$, since any adatom in a given PLG site can switch KLG sublattices without affecting the energy. The PLG (2.2) reduces to an ordinary lattice gas.[13] An Ising-type[14] critical point occurs at $K_c = \ln 3$, $\Delta_c = 3K_c + \ln 3$. A semi-infinite line, $\Delta = 3K + \ln 3 > \Delta_c$, of first-order transitions separates a "liquid" (dense: $n > \frac{1}{2}$) phase at low Δ and a "gas" (dilute: $n < \frac{1}{2}$) phase at high Δ.

2. Pure three-state Potts region. In the $\Delta \ll -1$ region, only the configurations ($t=1, s$) with no vacancy contribute non-negligibly to the averages (2.4). Then only the J term in (2.2) is of any importance, and the PLG reduces to the pure three-state Potts model.[18] A higher-order[17] transition occurs at[18] $3J_{P3} = \ln[1 + \sqrt{3}/(2\cos 10°)]$, separating a liquid ($n=1$, $n_a = n_b = n_c$) phase at low J and three coexisting "in-registry solid" ($n=1$, $n_a > n_b = n_c$ and permutations) phases at high J.

3. Four-state Potts line. On the line $J = \frac{1}{4}K = \frac{1}{18}\Delta$, the PLG Hamiltonian (2.2) reduces to

$$-\beta \mathcal{H} = 3J \sum_{\langle ij \rangle} (\delta_{u_i u_j} - 1), \quad u_i = 0, a, b, \text{ or } c, \tag{2.6}$$

which corresponds to the four-state Potts model.[18] A higher-order[17] transition occurs at[18] $J_{P4} = \frac{1}{3}\ln 2$, separating a liquid ($n = \frac{3}{4}$, $n_a = n_b = n_c$) phase at low J and four coexisting phases at high J. These coexisting phases are a gas ($n < \frac{3}{4}$, $n_a = n_b = n_c$) and three in-registry solids ($n > \frac{3}{4}$, $n_a > n_b = n_c$ and permutations).

4. Asymptotic first-order transition. In the region $\Delta \gtrsim 6J + 3K \gg 1$, the state ($t=0$) with all PLG sites vacant completely dominates the averages (2.4), while at $\Delta \lesssim 6J + 3K \gg 1$, the states with all PLG sites occupied at the same KLG sublattice, e.g., ($t=1$, $s=a$), completely dominate. Domination abruptly shifts at the equality, constituting a first-order phase transition between a gas ($n=0$) phase and three coexisting in-registry solid (n_a, n_b, or $n_c = 1$) phases.

C. Migdal recursion relations for triangular lattice

The renormalization-group approach[23] consists of the stepwise solution of a statistical problem, by a recursive elimination of degrees of freedom, as illustrated below. One version[21,22] of this approach, treating the position-space representation of the partition function, is especially suited to two-dimensional lattice problems. An exact treatment is usually impossible, because arbitrary types of further-neighbor, many-site interactions are generated. Therefore, one resorts to uncontrolled approximations (no apparent small parameter), which nevertheless have proven to be remarkably successful.

Migdal[29] has introduced an approximate position-space renormalization-group transformation which

has a simple, yet quite useful[31,38,39] form. This transformation was shown by Kadanoff[30] to also result from a potential-moving[22] approximation. Migdal's procedure was developed for, and to date used on, hypercubic lattices. We now adapt it to the triangular lattice. View the entire PLG lattice as composed of adjacent "supertriangles," each involving six sites. Two such adjacent supertriangles are shown on the left side of Fig. 4. The supertriangles, being adjacent, share sides, so each site participates in either two, or six (if at vertices) supertriangles. As the first step of our transformation, the bonds inside the supertriangles are moved to their perimeters. A special concern here, unconnected with the lattice type, is the single-site interaction Δ. As can be seen in Secs. III B 3 and in III B 4, important features of the PLG phase diagram are directly affected by the ratio of the single-site and nearest-neighbor interaction constants. To keep this ratio intact at each site, we rewrite the PLG Hamiltonian (2.2) as

$$-\beta\mathcal{H}=-\beta\sum_{\langle ij\rangle}\mathcal{H}_{ij}\,,$$
$$-\beta\mathcal{H}_{ij}=J(3\delta_{s_is_j}-1)t_it_j+Kt_it_j-\tfrac{1}{6}\Delta(t_i+t_j)\,, \tag{2.7}$$

and take $-\beta\mathcal{H}_{ij}$ to be the bond, moved in its entirety. Treating Δ on the same footing as J and K also avoids an arbitrariness resulting from parameterization, because one could redefine[24,37] the local variables (t,s) and thereby scramble single-site and nearest-neighbor couplings. This single-site interaction-moving scheme was also arrived at, from different considerations, in previous work.[39] Thus, at the completion of our first, potential-moving step, the PLG sites are coupled only along the supertriangle perimeters (middle of Fig. 4):

$$-\beta\tilde{\mathcal{H}}=-\beta\sum_{\langle ij\rangle}^{P}[\tilde{J}(3\delta_{s_is_j}-1)t_it_j+\tilde{K}t_it_j-\tfrac{1}{6}\tilde{\Delta}(t_i+t_j)]\,, \tag{2.8}$$
$$\tilde{J}=bJ\,,\quad \tilde{K}=bK\,,\quad \tilde{\Delta}=b\Delta$$

where P indicates summation over peripheral nearest-neighbor pairs only, and for the present example $b=2$, as can be checked by comparing the numbers of moved and unmoved bonds (also seen easily by imagining the bonds moved perpendicularly to their direction without changing this direction).

The second step is a dedecoration[40]: All sites not at supertriangle vertices are eliminated by summing over their variables (t,s) in the partition function (2.5). This induces renormalized

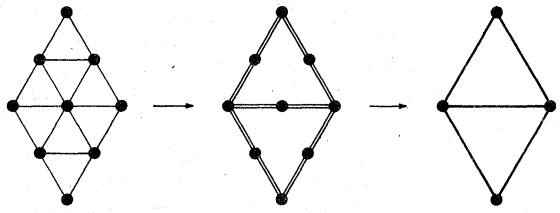

FIG. 4. Migdal's renormalization-group transformation adapted to the triangular lattice (Sec. II C). The case of length-rescaling factor $b=2$ is shown here, but the transformation can be performed with arbitrary b.

interactions, $J'=J'(J,K,\Delta)$, etc., between the vertex sites, as expressed with the recursion relations

$$J'=\tfrac{1}{3}\ln\frac{R_3}{R_4}\,,\quad K'=\tfrac{1}{3}\ln\frac{R_1^3R_3R_4^2}{R_2^6}\,,\quad \Delta'=6\ln\frac{R_1}{R_2}\,,$$
$$R_1=1+3z^2\,,\quad R_3=z^2+(2x^{-2}+x^4)y^2z^4\,, \tag{2.9}$$
$$R_2=z+(2x^{-1}+x^2)yz^3\,,\quad R_4=z^2+(x^{-2}+2x)y^2z^4\,,$$
$$x\equiv e^{bJ}\,,\quad y\equiv e^{bK}\,,\quad z\equiv e^{-b\Delta/6}\,.$$

This completes the renormalization-group transformation. The starting PLG has been mapped onto a new PLG involving only what were the supertriangle-vertex sites (right-hand side of Fig. 4). The structure of the problem (kinematics, coupling types) is preserved, whereas the length scale is increased by a factor $b=2$, and the interaction constants are renormalized. This transformation can be performed with arbitrary length-rescaling factor b by choosing supertriangles involving $\frac{1}{2}(b+1)(b+2)$ sites. Equation (2.8) is valid for arbitrary b; (2.9) was readily generalized to an arbitrary number $(b-1)$ of dedecorations by diagonalizing a 4×4 transfer matrix. Unlike the case of hypercubic lattices,[30] this Migdal transformation does not break the symmetry of the triangular lattice.

Our results in Sec. III are obtained with the $b=2$ recursion relations (2.9). The methodology for arriving at a global, multicritical phase diagram, once a position-space renormalization-group transformation is developed, is detailed elsewhere.[24] We briefly recall how densities are evaluated[41]: Let $\{n_\alpha\}$ be the set of generalized densities adjoint to the interaction constants $\{K_\alpha\}$, so that

$$n_\alpha=\frac{1}{N}\frac{\partial}{\partial K_\alpha}\ln Z\,, \tag{2.10}$$

N being the number of PLG sites. Specifically, $n\equiv\langle t_i\rangle=-n_\Delta$. For a single step (2.9), $K'_\alpha=K'_\alpha(K_\beta)$, in a renormalization-group trajectory, the den-

TABLE II. The PLG higher-order fixed points produced by the renormalization-group transformation developed in Sec. II C. Exact or conjectured values, referenced in the text, are given in parentheses for comparison. See Figs. 5 and 8 for the fixed-point connectivity, and Sec. III A for an overall discussion.

Higher-order fixed point: type	Location J^*, K^*, Δ^* (exact)	Eigenvalue exponents y_α (exact or conjectured) Even: y_2, y_4, y_6	Odd: y_1, y_3, y_5
	1. Finite-coupling		
C^*: Ising critical	0, 1.262, $3K^*+1.037$ (0, 1.099, $3K^*+1.099$) [a]	1.8746, 0.77, $-\infty$ (1.875, 1) [c]	1, −0.52, $-\infty$
P_4^*: Four-state Potts	0.252, $4J^*$, $18J^*$ (0.231, $4J^*$, $18J^*$) [a]	1.860, 0.89, 0.58 (1.875, 1.5) [c]	1.860, 0.58, 0.35 (1.875) [c]
B^*: Fourth-order	0.431, −0.151, 1.580	1.489, 0.23, −1.43 (1.5) [d]	1.896, 0.61, −0.32 (1.875) [d]
	2. Strong-coupling		
P_3^*: Three-state Potts (tricritical)	0.231, −0.057, $-\infty$ (0.210) [a]	0.83, −1, $-\infty$	1.868, 0.55, 0 (1.875) [c]
P_{3E}^*: Potts tricritical end-point	0.231, ∞, $3K^*+1.504$ (0.210) [b]	2, 0.83, −1 (2) [c]	1.868, 0.55, 0.50 (1.875) [c]

[a] Section II B.
[b] Obtained by combining the arguments of Secs. II B 1 and II B 2.
[c] Section III A.
[d] Section III C.

sity recursion relation is derived by the chain rule

$$n_\alpha = \frac{1}{b^d} \sum_\beta n'_\beta \frac{\partial K'_\beta}{\partial K_\alpha} \ . \tag{2.11}$$

The densities at a given initial point in interaction-constant space are evaluated by iterating (2.11) until a phase-sink[24] fixed point, with obvious $\{n_\alpha^*\}$, is virtually reached.

III. RESULTS

A. Global phase diagram of the Potts lattice gas

Our renormalization-group transformation produced thirteen fixed points for the $J, K \geq 0$ quadrants of J, K, Δ space. These fixed points are classified in Tables II and III, and their locations and higher-order eigenvalue exponents are given. The odd (magnetic-field-like) eigenvalue expo-

TABLE III. The PLG first-order and trivial fixed points. The classification scheme of Ref. 24 is used. See Fig. 5 for the fixed-point connectivity.

	Type	Location J^*, K^*, Δ^*	Domain
		1. First-order fixed points	
So^*	Discontinuous $n_a - n_b$ Three-solid coexistence	∞, ln3 − $2J^*$, $-\infty$ $-\Delta^* \gg J^*$	Volume
$F_{4\pm}^*$, F_{40}^*	Discontinuous $n_a - n_b, n$ Three-solid, gas coexistence	$\infty, 4J^*+A^*, 6J^*+3K^*$ $J^* \gg \lvert A^* = \pm\infty, 0 \rvert$	Surface
F_2^*	Discontinuous n Liquid, gas coexistence	$0, \infty, 3K^*+\ln 3$	Surface
		2. Trivial fixed points	
Li^*	Liquid sink	$0, 0, -\infty$	Volume
Ga^*	Gas sink	$0, 0, +\infty$	Volume
S^*	Smooth continuation between liquid and gas	0, 0, 0	Surface

nents are obtained by adding the symmetry-breaking perturbations

$$-\beta\mathcal{H}_{\text{odd}} = H\sum_i t_i \delta_{s_i a} + \sum_{\langle ij\rangle} t_i t_j [L(\delta_{s_i a} + \delta_{s_j a}) + M\delta_{s_i a}\delta_{s_j a}] \quad (3.1)$$

to the Hamiltonian (2.2). The fixed-point connectivity is shown in Fig. 5. The resulting phase diagram[32] is shown in Fig. 6. The combinations $1/J$, Δ/J, and K/J were chosen as phase-diagram axes, because the former two are, respectively, proportional [see Eq. (2.2)] to temperature and chemical potential,[34] and the latter is fixed, through (2.3), by the ratio of adsorbate diameter to graphite site separation. This phase diagram reproduces all the features derived in Sec. II B (except the precise transition temperatures, see Table II and discussion below).

The $J, K \geq 0$ quadrants of interaction space are portioned [42,43] into three coexisting "in-registry solid" ($n \to 1$, $n_a > n_b = n_c$ and permutations) phases at high chemical potential ($-\Delta/J$) and low temperature ($1/J$), a "liquid" ($n \to 1$, $n_a = n_b = n_c$) phase at high chemical potential and high temperature, and a "gas" ($n \to 0$, $n_a = n_b = n_c$) phase at low chemical potential (see Fig. 6). The solid is separated from the liquid by the surface $P_3^{(0)}B^{(0)}P_4P_{3E}^{(\infty)}P_3^{(\infty)}$ of Potts tricritical[16,17,24] points, and from the gas by the surface $F_4^{(0)}B^{(0)}P_4P_{3E}^{(\infty)}F_4^{(\infty)}$ of first-order transitions, a locus of four-phase coexistence. These two surfaces are separated at $K/J<4$ by the line $B^{(0)}P_4$ of fourth-order points, and at $K/J>4$ by the line $P_4P_{3E}^{(\infty)}$ of Potts tricritical end-points. (Parenthesized superscripts give K/J values, when necessary.) At $K/J<4$, the liquid and gas phases smoothly join into one "fluid" phase, with no intervening phase transition. At $K/J>4$, these two phases are separated by the surface $P_{3E}^{(\infty)}P_4C^{(\infty)}$ of first-order transitions, this surface being bounded by the line $P_4C^{(\infty)}$ of Ising critical (second-order) points, beyond which the two phases again smoothly join into one fluid phase. (In this region, in fact, constant K/J cross sections of our phase diagram are like[44] the familiar phase diagrams[2] of bulk solid-fluid systems, except that the solid-liquid transition is higher-order.) The three lines singled out in this description meet, at $K/J=4$, $\Delta/J=18$, at the four-state Potts transition point P_4 [Sec. II B 3].

The Ising critical (C^*), three-state Potts (P_3^*) and four-state Potts (P_4^*) fixed points occur in the respective regions in which these transitions were identified in Sec. II B (the domains of C^* and P_3^* do extend these transitions outside these regions).

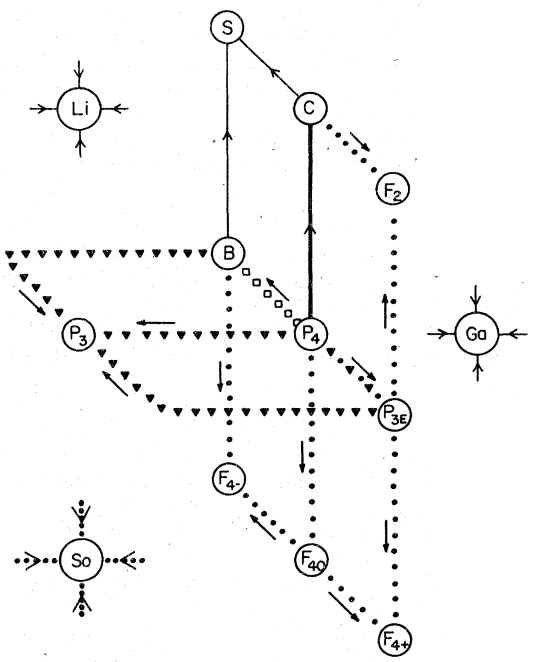

FIG. 5. Fixed-point connectivity. Renormalization-group trajectories flowing through the various types of phase boundaries are indicated: first-order (●●●), Ising critical (dark line), Potts tricritical (▼▼▼), Potts tricritical end-point (▼●▼), and fourth-order (□□□). Light trajectories do not coincide with any phase transition.

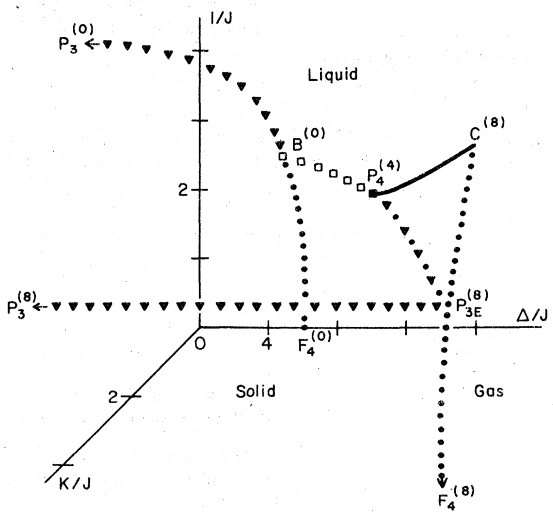

FIG. 6. PLG global phase diagram (Sec. III A). The $K/J=0,8$ cross sections, and the special lines connecting them are shown. Parenthesized superscripts give K/J values. First-order (●●●), Ising critical (dark line), Potts tricritical (▼▼▼), Potts tricritical end-point (▼●▼), fourth-order (□□□), and four-state Potts (■) transitions are indicated.

Thus, we know the accuracy of these fixed-point locations: $K_C^*, J_{P3}^*, J_{P4}^*$ are, respectively, 15%, 10%, and 9% away from the exact values[14,18] given in Sec. IIB. At the Ising critical fixed point, Δ_C^* is off by -1% from the exact relation $\Delta_C^* = 3K_C^* + \ln 3$; this is because our approximate renormalization-group transformation does not conserve the empty $\longleftrightarrow$ occupied ($l = 0 \longleftrightarrow 1$) symmetry of the ordinary lattice-gas problem. On the other hand, at the four-state Potts fixed point, $J_{P4}^* = \frac{1}{4}K_{P4}^* = \frac{1}{18}\Delta_{P4}^*$ as in Sec. IIB 3, because our approximation conserves the symmetry resulting from permuting[24,37] the labels (0, a, b, c) of the four states of a PLG site.

The largest eigenvalue exponents, as usual,[21,24] turned out to be the most accurate quantities of our approximate treatment. These are $y_2(C^*)$, $y_1(P_3^*)$, and $y_2(P_4^*)$, which are identified as the magnetic eigenvalue exponents $y_H(q)$ of the $q = 2$ (Ising), 3, and 4-state Potts models.[18] According to Suzuki's new universality hypothesis,[45] $y_H(q = 3, 4)$ could be equal to the exactly known[14] $y_H(q = 2) = \frac{15}{8}$. This is supported by series[46,47] and renormalization-group[24,48,49] calculations. In our present calculation, $y_2(C^*)$, $y_1(P_3^*)$, and $y_2(P_4^*)$ indeed, respectively, deviate by only 2, 38, and 78 parts in 10^4 from $\frac{15}{8}$.

The next-largest eigenvalue exponents, $y_4(C^*)$, $y_2(P_3^*)$, and $y_4(P_4^*)$, are identified as the thermal eigenvalue exponents $y_T(q)$ of the $q = 2$, 3, and 4-state Potts models. The Ising $y_4(C^*) = 0.77$ is below the exact value[14] of 1. Similarly, $y_2(P_3^*) = 0.83$ and $y_4(P_4^*) = 0.89$ are below the values of 1.20 and 1.32 obtained in more accurate variational renormalization-group calculations,[48-50] and below the conjectured $y_T(q = 4)$ value[47] of $\frac{3}{2}$. Our values do reproduce the trend of $y_T(q)$ increasing with q: $y_T(q) > y_T(q-1)$. When this inequality is taken in conjunction with the correct[14] $y_T(q = 2) = 1$, an increasingly positive specific-heat exponent[2] $\alpha = 2 - d/y_T$, where $d = 2$ is dimensionality, results for $q = 3, 4$.

At our four-state Potts fixed point P_4^*, each of the two even eigenvalue exponents corresponding to deviations from the four-state Potts subspace ($J = \frac{1}{4}K = \frac{1}{18}\Delta$) exactly equals an odd eigenvalue exponent: $y_2 = y_1$ and $y_6 = y_3$. A proof for this type of degeneracy has been given.[24] The smaller positive, odd exponent at the Potts tricritical fixed point P_3^*, $y_3 = 0.55$, is to be compared with the values 0.52 and 0.46 obtained in previous renormalization-group studies.[24,48] The fixed point P_{3E}^* for the Potts tricritical end-points has exactly the same relevant (positive) eigenvalue exponents as P_3^*, and also the eigenvalue exponent $y_2 = 2 =$ dimensionality, necessary for a first-order transition.[51] This is in accord with the renormalization-group mechanism[24] for end-point behavior.

The asymptotic first-order phase boundaries derived in Sec. IIB are reproduced: $\Delta = 3K + \ln 3 \gg 1$, $J = 0$ at F_2^*, and $\Delta = 6J + 3K \gg 1$ at $F_{4\pm}^*, F_{40}^*$. The density $(n_a - n_b)$ is discontinuous at the domains of So^*, $F_{4\pm}^*, F_{40}^*$. This density is the average value of the local operator $t_i(\delta_{s_i a} - \delta_{s_i b})$, which constitutes an "odd" interaction, i.e. an interaction breaking the (a, b, c) permutation symmetry, as in (3.1). Accordingly, the first-order fixed points So^*, $F_{4\pm}^*, F_{40}^*$ have their leading odd eigenvalue exponent y_1 equal to 2, the dimensionality.[51] The density n is discontinuous at the domains of $F_{4\pm}^*$, F_{40}^*, F_2^*, and P_{3E}^*. The corresponding operator t_i constitutes an "even" interaction [the $-\Delta\sum_i t_i$ term in (2.2)], which does not break the (a, b, c) permutation symmetry. The latter first-order fixed points have their leading even eigenvalue exponent y_2 equal to 2.

We have deferred until Sec. IIIC the discussion of the fixed point B^*, which controls the fourth-order line $B^{(0)}P_4$.

B. Krypton submonolayer phase diagram

Eq. (2.3), connecting the PLG Hamiltonian (2.2) and the Lennard-Jones (LJ) potential (2.1) between krypton adatoms,[8] reduces to

$$K/J = 2.10\,, \tag{3.2a}$$

$$1/J = T/32.8\,, \tag{3.2b}$$

where the temperature T is in degrees Kelvin. The right-hand side of (3.2a) is entirely determined by the ratio of the adatom LJ diameter σ to the graphite site separation a. Equation (3.2a) selects a cross section of the global phase diagram in Fig. 6 as applicable to krypton submonolayers. Eq. (3.2b), determined by both σ/a and the LJ well depth ϵ, sets the temperature scale.

The resulting temperature versus chemical potential[34] ($-\Delta/J$) phase diagram for krypton submonolayers is shown in Fig. 2(a). Three coexisting in-registry solid[42] ($n \to 1$, $n_a > n_b = n_c$ and permutations) phases occupy the low-temperature high-chemical-potential region. These are separated, by the line P_3B of Potts tricritical points, from the liquid[42] ($n \to 1$, $n_a = n_b = n_c$) phase of the high-temperature, high-chemical-potential region. The solids are separated, by the line F_4B of first-order transitions, from the gas[42] ($n \to 0$, $n_a = n_b = n_c$) phase of the low-chemical-potential region. On the latter line, the three solids and the gas coexist. These four phases become indistinguishable at the point B, which is therefore a fourth-order transition point. In this diagram, the liquid and gas phases connect smoothly, without any intervening phase transition (in contrast to Fig. 9).

The temperature versus density ($n \equiv \langle t_i \rangle$) version of the krypton submonolayer phase diagram results from evaluating[41] n at the phase boundaries mentioned above, and is shown in Fig. 2(b). At higher temperatures, again the Potts tricritical line P_3B separates the three coexisting solid phases from the liquid phase. At lower temperatures, a "phase-separation" region F_SBF_G separates the solid phases from the gas phase: A given temperature, density point inside F_SBF_G represents a system which actually has separated into solid and gas domains, at respective densities determined by drawing a constant-temperature [in Fig. 2(b), horizontal] line to the two "branches" F_SB and F_GB of the phase-separation boundary. Again, this means a four-phase coexistence inside F_SBF_G, terminating at the fourth-order point B.

This temperature versus density phase diagram provides direct comparison between experimental data on the krypton-graphite system and the position-space renormalization-group treatment of our idealized system: Points from the vapor-pressure experiments of three groups[6-8] are shown in Fig. 2(b). These span both tricritical and first-order regions, implying[8] the existence of the fourth-order point in between (Sec. IIIC).

The branch $(F_SB)_{\text{expt}}$ of the phase-separation boundary, deducible from the experimental points, occurs at lower coverage and is much steeper, almost vertical, in Fig. 2(b). This discrepancy may be due to second-layer adsorption[6,8] or, possibly, due to defects of the graphite substrate.[52]

As deduced from Thomy and Duval's[6] original data [dark circles in Fig. 2(b)], the other branch $(F_GB)_{\text{expt}}$ departs from our theoretical curve in a different manner. Let us follow this $(F_GB)_{\text{expt}}$ as the density n increases from zero to $(n_B)_{\text{expt}} \simeq 0.85$. The boundary temperature first increases similarly to our curve, but evidently undergoes a broad maximum at $n \sim 0.43$ and proceeds to decrease. Further on, at $n \sim 0.69$, it undergoes a minimum and increases to T_B. This amounts to distinct liquid and gas phases on each side of the maximum, separated by a first-order transition. The tip of the maximum is an isolated critical point, presumably Ising type, and the tip of the minimum is a solid-liquid-gas coexistence point, an analog of the bulk triple point. The liquid "valley" spans a temperature interval of 9 °K, with the triple point at 77 °K. Thomy and Duval presented[6] this low-temperature, low-density data in analogy to the bulk-krypton phase diagram. Subsequently, Larher[7] scanned the low-temperature region. His data (open circles) does not explicitly exhibit decreasing temperature of the low-density branch with increasing density. Extrapolation of this data implies a liquid valley spanning a temperature interval of less than 2 °K, the triple point occurring at 85 °K. Our present work cannot claim to determine the existence or nonexistence of such liquid-valley, triple-point structure: If it exists, our approach, at the present level of approximation, probably would miss it, because our renormalization-group flows are in an (only) three-parameter space [however, in Fig. 9, see a similar structure for a different ($K/J > 4$) regime of our calculation]. But, if the krypton lattice gas does have this structure, this should be recovered by our approach carried to a higher level of approximation with higher-dimensional renormalization-group flows. Finally, we mention specific-heat data on nitrogen[12] and, recently, on krypton[9] adsorbed onto graphite, and the Monte Carlo study[53a] of a triangular lattice model with nearest-neighbor repulsion and next-nearest-neighbor attraction. These do not exhibit a liquid-valley, triple-point structure, but a phase boundary like ours. On the other hand, another triangular lattice model[53b] with nearest-neighbor exclusion and infinitely weak, infinitely long-ranged (Kac) attraction does have the triple point, but no multicritical structure.

We turn our attention to the line P_3B of Potts tricritical phase transitions, separating the solids from the liquid. Its $n = 1$ intercept P_3 should move to infinite temperature as the PLG is made to better represent the KLG, by taking into account inter-PLG-site nearest-neighbor exclusion. However, at $n \lesssim 1$, the KLG itself is a poor representation of adsorbed krypton. Second-layer formation[6,8] and behavior incommensurate[33] with the graphite substrate are experimentally known to occur. The experimental phase diagram continues to values greater than unity of the density n as defined here, with finite-temperature phase transitions involving layers compressed from the in-registry structure considered in this work. Away from the $n = 1$ axis, the slopes of our curve and of the experimental points[6,8] are in good agreement. The slight upward concavity[54] ($d^2T/dn^2 > 0$) of our curve is also seen in the data of Putnam and Fort[8] (open triangles). Our curve is displaced from the experimental points by about 17% towards high temperature. Previous authors[20] have noted the quantitative difficulty of constructing a phase-transition model from a LJ potential, due to the steepness of this potential at short distances. Besides, our present treatment is a low-level approximation with no adjustable parameter, and any agreement in transition temperatures much better than the 17% quoted above would be fortuitous. The LJ potential itself is only an approximate description of the microscopic situation, and it would be worthwhile to match our PLG

approach to a more refined potential.

The experimentally accessible tricritical exponents at P_3B are determined unfortunately by our inaccurate subdominant eigenvalue exponents [see discussion of $y(P_3^*)$ in Sec. III A]. Thus we obtain a negative specific-heat exponent $\alpha = 2 - d/y_2 = -0.41$, whereas best estimates are $\alpha = 0.33$ from variational renormalization groups,[48,49] 0.42 ± 0.05 from series expansion,[55] and 0.36 ± 0.02 from the transition of helium monolayers on graphite.[4] For the isothermal density singularities

$$|n - n_3| \sim |\mu - \mu_3|^{\beta_{22}} \quad \text{as} \quad \mu \to \mu_3 , \tag{3.3a}$$

$$(n_a - n_b) \sim (\mu - \mu_3)^{\beta_{12}} \quad \text{as} \quad \mu \gtrless \mu_3 , \tag{3.3b}$$

where n_3 and μ_3 are the density and chemical potential at the transition, we obtain the exponents

$$\begin{aligned} \beta_{22} &= [d - y_2(P_3^*)]/y_2(P_3^*) = 1.41 , \\ \beta_{12} &= [d - y_1(P_3^*)]/y_2(P_3^*) = 0.159 . \end{aligned} \tag{3.4}$$

Using $y_1 = \frac{15}{8}$, $y_2 = d/(2 - \alpha)$, and the α values[4,48,49,55] quoted above, the correct β_{22} is estimated between 0.53 and 0.67, and the correct β_{12} between 0.096 and 0.104.

C. Fourth-order transition point B

The fourth-order transition point B appearing in the krypton submonolayer phase diagrams of Fig. 2 is the intersection of the "krypton plane" $K/J = 2.10$ [Eq. (3.2a)] with the fourth-order line $B^{(0)}P_4$ of the global phase diagram of Fig. 6. This point occurs at $\Delta_B/J_B = 11.8$, $T_B = 108\,^{\circ}\mathrm{K}$, and $n_B = 0.747$. Extrapolation from the phase-boundary points proposed by Thomy and Duval[6] gives $(T_B)_{\text{expt}} = 98\,^{\circ}\mathrm{K}$ and $(n_B)_{\text{expt}} = 0.853$. However, examination of the vapor-pressure isotherm points in this reference suggests $89\,^{\circ}\mathrm{K} < (T_B)_{\text{expt}} < 98\,^{\circ}\mathrm{K}$. Indeed, Putnam and Fort[8] observed a continuous transition at $T = 95\,^{\circ}\mathrm{K}$, $n = 0.798$.

In discussing the point B, we first mention another model defined on a triangular lattice, the triplet Ising model (TIM):

$$-\beta \mathcal{H}_{\text{TIM}} = R \sum_{\langle ijk \rangle} s_i s_j s_k , \quad s_i = \pm 1 . \tag{3.5}$$

Ths sum is over all nearest-neighbor triplets of sites, and we take R non-negative. The TIM was solved exactly by Baxter and Wu.[26] It has a continuous phase transition at $R_B = \frac{1}{2}\ln(1 + \sqrt{2})$, between a high-temperature ($R < R_B$) phase and four coexisting low-temperature ($R > R_B$) phases. The ground state of each low-temperature phase is shown in Fig. 7(a), where $s_i = +1(-1)$ is now defined to mean occupied (empty). Each of three low-temperature phases has one triangular sublattice predominantly occupied and two triangular

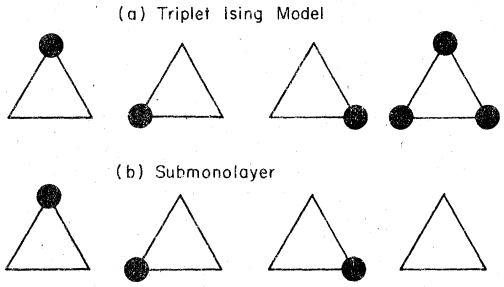

FIG. 7. Ground states of coexisting low-temperature phases (Sec. III C). Occupied sites are shown with dark circles. Each site in this figure exhibits the occupation state of its entire sublattice.

sublattices predominantly empty; the other low-temperature phase has all three sublattices predominantly occupied. The transition at R_B is a fourth-order transition, since the four coexisting $R > R_B$ phases continuously become indistinguishable. Two exponents at R_B are[26] $\alpha = \frac{2}{3}$ (exact) and $\beta = \frac{1}{12}$ (conjectured). These correspond to thermal and magnetic eigenvalue exponents $y_T(\text{TIM}) = \frac{3}{2}$ and $y_H(\text{TIM}) = \frac{15}{8}$.

Returning to the krypton submonolayer problem, consider the leading even and odd eigenvalue exponents of B^*, the fixed point which produces the singularities of the fourth-order transition at B,

$$y_2(B^*) = 1.489 \tag{3.6a}$$

is -0.7% off $y_T(\text{TIM})$, and

$$y_1(B^*) = 1.896 \tag{3.6b}$$

is 1.1% off $y_H(\text{TIM})$. To appreciate the meaning of these numbers resulting from an approximate calculation, consider all three of our finite-coupling, higher-order fixed points, shown in Fig. 8. They occur consecutively as B^*, P_4^*, and C^* on a crossover line, and exhibit analogous eigendirection structures. The analogs of $y_2(B^*)$ are $y_2(P_4^*)$ and $y_2(C^*)$, which are -0.8% and -0.02% off their expected values, respectively (Sec. III A). One analog of $y_1(B^*)$ is the neighboring $y_1(P_4^*)$, which is again -0.8% off its expected value. [No expected value is available for $y_1(C^*)$, probably a redundant[24,56] exponent.] We conclude the following:

(i) As far as these eigenvalue exponents are concerned, it is reasonable to assign a 1% accuracy to our calculation.[57]

(ii) Therefore, the relations

$$y_2(B^*) \stackrel{?}{=} y_T(\text{TIM}) = \tfrac{3}{2} , \tag{3.7a}$$

$$y_1(B^*) \stackrel{?}{=} y_H(\text{TIM}) = \tfrac{15}{8} \tag{3.7b}$$

are probably correct. The latter eigenvalue exponent is seen in several two-dimensional sys-

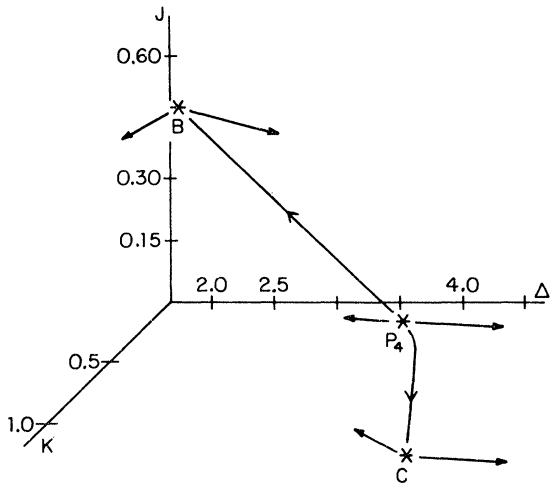

FIG. 8. Finite-coupling, higher-order fixed points, and the crossover flow line connecting them. The Ising critical C^* is in the $J=0$ plane, the fourth-order B^* is slightly behind the $K=0$ plane, $K(B^*)=-0.151$, and the four-state Potts P_4^* is inside the quadrant shown. The long and short arrows at each fixed point are the eigendirections of the dominant y_2 and subdominant y_4 eigenvalue exponents.

tems (as predicted by Suzuki's new universality,[45] Sec. III A), but the equality (3.7a) would be quite remarkable.

To continue the comparison between the fourth-order points in the TIM and the submonolayer problem, we recall the four low-temperature phases which coexist at the first-order line F_4B in Fig. 2(a), and which become indistinguishable (achieve fourfold criticality) at B. These are the three in-registry solids and the gas. The ground state of each is shown in Fig. 7(b). Each solid has one sublattice predominantly occupied and two sublattices predominantly empty; the gas has all three sublattices predominantly empty. The three solids map onto each other under the symmetries of the triangular lattice, while the gas remains invariant. The three analogous phases of the TIM also map onto each other under the symmetries of the triangular lattice, while the other phase remains invariant. However, the TIM phases actually have a higher symmetry: The Hamiltonian (3.5) is invariant under the transformation which flips all spins on two sublattices. Together with the symmetries of the triangular lattice, this makes it possible to arbitrarily permute the definitions of any two low-temperature phases. This is the symmetry of the four-state Potts model.[18,58] In fact, the conjectured exponents[47] of the four-state Potts model equal the TIM ones. Thus, these two models should be in the same universality class.[59]

The higher, fourfold symmetry is not manifest in the submonolayer problem. In the TIM, one consequence of this symmetry is that at the transition the nearest-neighbor triplets are equally distributed between the configurations shown in Fig. 7(a). The analogous statement, with the configurations in Fig. 7(b), is fulfilled to 1% at the submonolayer point B. More generally, if the fourfold symmetry were present in the submonolayer problem, the density relation

$$n(\text{gas}) = 3[1 - n(\text{solid})] \tag{3.8}$$

would hold, at any given temperature, at the coexistence boundary. Eq. (3.8) is satisfied to better than 3% in our calculation. Finally, in puzzling contrast to the TIM, our four-phase coexistence trajectory does not leave B^* along the direction of the even eigenvalue $y_2 = 1.5$, but asymptotically along the direction of the subdominant even eigenvalue $y_4 = 0.23$.

The occurrence in the submonolayer phase diagram of the fourth-order point B has several relevant consequences. This point is certainly in a universality class different from that of the line of continuous transitions it terminates. The large specific-heat exponent $\alpha = \frac{2}{3}$ could be measured [we tentatively use the values in (3.7) rather than (3.6)]. Crossover to this large value should be noticed as the Potts tricritical line P_3B is approached at decreasing densities n. The isothermal ($T = T_B$) density singularities have the exponents $\beta_{22} = [d - y_2(B^*)]/y_2(B^*) = \frac{1}{3}$ for the overall occupation (3.3a), and $\beta_{12} = [d - y_1(B^*)]/y_2(B^*) = \frac{1}{12}$ for the preferential occupation (3.3b), as distinct from the respectively estimated ~0.6 and ~0.10 at the tricritical line. Overall occupation is observed in vapor-pressure experiments.[6-8] Preferential occupation could be observed by neutron[10] and low-energy electron[60] diffraction. Another experimentally verifiable result of our treatment is that the two branches F_SB and F_GB of the phase-separation boundary [Fig. 2(b)] form a cusp at B, given by

$$[n(\text{solid}) - n(\text{gas})]_T \sim [(T_B - T)/T_B]^{\beta_{24}}, \tag{3.9}$$

where

$$\beta_{24} = [d - y_2(B^*)]/y_4(B^*) = 2.2 .$$

Unfortunately, this value probably is very inaccurately large, because $y_4(B^*) = 0.23$ has the consecutive analogs $y_4(P_4^*)$ and $y_4(C^*)$, which deviate, respectively, by −41% from the conjectured value[47] and by −23% from the exact value.[14] If the correct $y_4(B^*)$ were larger than $\frac{1}{2}$, the cusp would be replaced by a rounded curve. This would be the case if, in analogy to (3.7), the correct $y_4(B^*)$ were equal to $\frac{7}{8}$, the conjectured value[61] of the

subdominant eigenvalue exponent[62] of the TIM. Then β_{24} would be $\frac{4}{7}$.

D. Other adsorbates and tricritical end-point behavior

Our model is in general applicable to any adsorbate whose adatom pair potential is qualitatively represented by Fig. 1(b). Quantitative contact is established as in Sec. II A, with equations like (2.3), only with different numbers inside the parentheses in the right-hand side. In each case, the ratio of the adatom LJ diameter σ to the graphite site separation a selects a constant K/J cross section of the global phase diagram in Fig. 6; both σ/a and the LJ well depth ϵ set the temperature scale.

We have applied this analysis to nitrogen, methane, and ethane, obtaining phase diagrams similar to the one in Fig. 2. The LJ parameters[63,64] which we used, the corresponding PLG parameters, and the resulting temperatures T_B of the fourth-order points are in Table IV. As best estimates, $(T_B)_{adj}$ are obtained by one overall adjustment of all the temperature scales, matching for krypton the experimental[6,8] T_B. The latter is taken in the range 89 to 98 °K (Sec. III C); corresponding $(T_B)_{adj}$ ranges for other adsorbates are in Table IV. Experimentally observed first-order and continuous transition temperatures constitute lower and upper bounds to T_B. Available results are given in Table IV. Our best estimate falls within these bounds for nitrogen,[12] but is still somewhat high for methane.[6] Neutron scattering[65] indicates that argon does not adsorb in-registry with basal graphite, and our model probably is not applicable. The third-neighbor potential[63] is most favorable in xenon adsorbed onto basal graphite. This qualitative dissimilarity to Fig. 1(b), or equivalently to the LJ entries in Table I, makes (2.3) unjustified: The meaning of J is dubious. So, again, our present treatment is not applicable. However, since xenon does form in-registry submonolayers,[60] a modification of our approach may be useful.

When the adatom second-neighbor pair potential is not much more negative than the third- and fourth-neighbor potentials, equations like (2.3) give K/J values greater than 4. These cross sections of the global phase diagram exhibit a tricritical end-point topology, as distinguished from the fourth-order point topology discussed above. This is illustrated with $K/J = 4.4$ in Fig. 9. In the temperature $(1/J)$ versus chemical potential (Δ/J) phase diagram, Fig. 9(a), the Potts tricritical[16-18] line separating the solids from the liquid terminates at the Potts tricritical end-point P_{3E}. No new critical exponent appears at this point.[24] The liquid and the gas are separated by the first-order line $P_{3E}C$, which terminates at the isolated Ising critical (second-order) point C. This phase diagram looks like[44] the familiar phase diagrams[2] of bulk solid-fluid systems, except that the solid-liquid transition is higher-order. In the temperature vs. density (n) phase diagram, Fig. 9(b), $F_S P_S P_G F_G$ is a phase-separation region with solid and gas domains, and $P_S C P_G$ is a phase-separation region with liquid and gas domains. $P_3 P_S P_G$ is a locus of Potts tricritical transitions, and C is the isolated critical point.

The use of a mixture of gases as adsorbate should be an experimental procedure for continuously varying an effective K/J value.[66] Thus, if an adsorbate having the tricritical end-point topology were discovered, one could also mix it

TABLE IV. The PLG model applied to various adsorbates (Sec. III D). Since no LJ parameters are available for adsorbed nitrogen, methane, and ethane, we made estimates: The LJ diameters σ are expected to be little different from the bulk cases (e.g., +1.9% for Ar and +1.0% for Xe in Ref. 63, and unchanged for Kr in Ref. 8), so the bulk σ were used for N_2, CH_4, and C_2H_6. The LJ well depth ϵ is depressed from the bulk value by 20.7% for Ar and 16.7% for Xe in Ref. 63, and by 15.2% for Kr in Ref. 8; the average of these numbers, 17.5%, was taken as the depression for N_2, CH_4, and C_2H_6.

	LJ parameters		PLG parameters		Fourth-order point temperatures/(°K)		
	σ/a	ϵ/k (°K)	K/J	$TJ/$(°K)	T_B	$(T_B)_{adj}$	Experiment
Ar	1.41[a]	95[a]	1.98	19.8	64	53 to 58	no registry[f]
Kr	1.46[b]	145[b]	2.10	32.8	108	89 to 98[b,e]	89 to 98[b,e]
N_2	1.50[c]	78[d]	2.23	22.0	61	50 to 55	50 to 65[g]
CH_4	1.55[c]	122[d]	2.50	32.9	94	77 to 84	? to 77[e]
C_2H_6	1.61[c]	200[d]	3.22	42.9	131	107 to 118	?

[a] Reference 63.
[b] Reference 8.
[c] Bulk σ from Ref. 64.
[d] Estimated as 82.5% of bulk ϵ from Ref. 64.
[e] Reference 6.
[f] Reference 65.
[g] Reference 12.

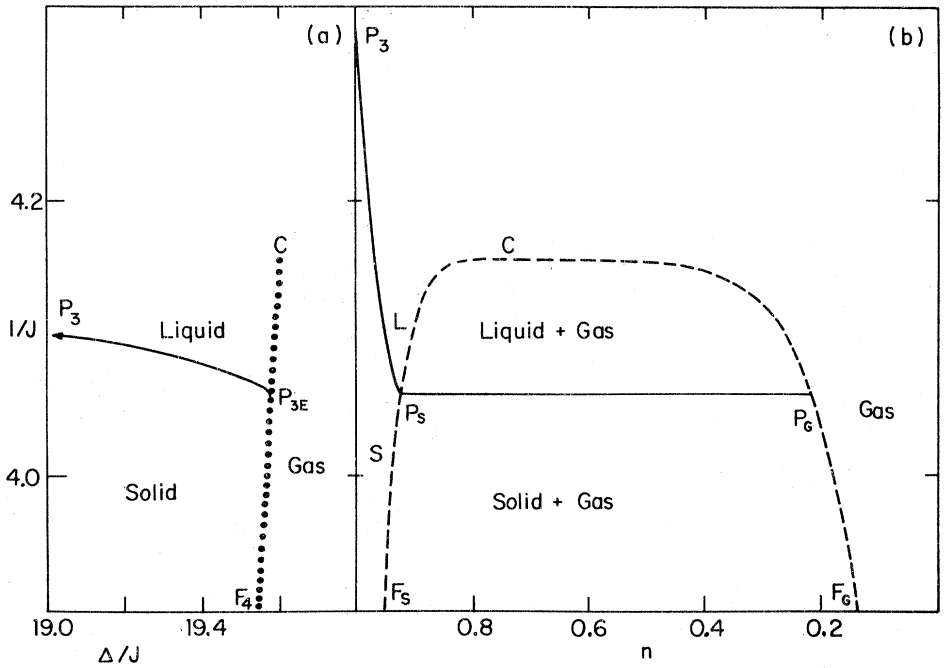

FIG. 9. Phase diagrams with Potts tricritical endpoint topology (Sec. III D), for $K/J = 4.4$. Full, dotted, and dashed lines, respectively, indicate Potts tricritical transitions, first-order transitions, and phase-separation boundaries. C is an isolated critical point. In diagram (b), S and L mark solid and liquid regions.

with for example krypton, to obtain an experimental realization[58,66] of the four-state Potts transition at effective $K/J = 4$.

ACKNOWLEDGMENTS

We have benefited from enjoyable discussions with Professors A. Aharony, H. Ehrenreich, R. B. Griffiths, P. C. Martin, and M. Wortis. We thank Professor B. I. Halperin and Dr. D. R. Nelson for reading our manuscript and providing most useful criticism. Two of the authors (A.N.B. and S.O.) are supported in part by the NSF under Grant No. NSF DMR-77-10210. One of us (F.A.P.) is supported by a Dupont Young Faculty Award.

[1]J. G. Dash, *Films on Solid Surfaces* (Academic, New York, 1975).

[2]For general reviews of phase transitions, see M. E. Fisher, Rep. Prog. Phys. 30, 615 (1967); L. P. Kadanoff *et al.*, Rev. Mod. Phys. 39, 395 (1967); H. E. Stanley, *Introduction to Phase Transitions and Critical Phenomena* (Oxford University, Oxford, 1971). A recent text including renormalization-group methods is S.-k. Ma, *Modern Theory of Critical Phenomena* (Benjamin, Reading, Mass., 1976).

[3]M. Bretz and J. G. Dash, Phys. Rev. Lett. 27, 647 (1971); M. Bretz, J. G. Dash, D. C. Hickernell, E. O. McLean, and O. E. Vilches, Phys. Rev. A 8, 1589 (1973); R. L. Elgin and D. L. Goodstein, *ibid.* 9, 2657 (1974).

[4]M. Bretz, Phys. Rev. Lett. 38, 501 (1977).

[5]G. B. Huff and J. G. Dash, J. Low Temp. Phys. 24, 155 (1976).

[6]A. Thomy and X. Duval, J. Chim. Phys. 66, 1966 (1969); 67, 286 (1970); 67, 1101 (1970).

[7]Y. Larher, J. Chem. Soc. Faraday Trans. 1 70, 320 (1974).

[8]F. A. Putnam and T. Fort, Jr., J. Phys. Chem. 79, 459 (1975); 81, 2164 (1977); F. A. Putnam, T. Fort, Jr., and R. B. Griffiths, *ibid.* 81, 2171 (1977); F. A. Putnam, Ph.D. thesis (Carnegie-Mellon University, 1976) (unpublished).

[9]G. A. Stewart, paper presented at the CNRS conference: Phases Bidimensionelles Adsorbées, Marseille, France (1977) (unpublished).

[10]J. K. Kjems, L. Passell, H. Taub, and J. G. Dash, Phys. Rev. Lett. 32, 724 (1974); J. K. Kjems, L. Passell, H. Taub, J. G. Dash, and A. D. Novaco, Phys. Rev. B 13, 1446 (1976).

[11]D. M. Butler, G. B. Huff, R. W. Toth, and G. A. Stewart, Phys. Rev. Lett. 35, 1718 (1975).

[12]T. T. Chung and J. G. Dash, Surf. Sci. 66, 559 (1977).

[13]C. N. Yang and T. D. Lee, Phys. Rev. 87, 410 (1952).

[14]L. Onsager, Phys. Rev. 65, 117 (1944); C. N. Yang, *ibid.* 85, 809 (1952); R. M. F. Houtappel, Physica (Utr.) 16, 425 (1950).

[15]C. E. Campbell and M. Schick, Phys. Rev. A 5, 1919 (1972).

[16]J. P. Straley and M. E. Fisher, J. Phys. A 6, 1310 (1973).

[17]R. J. Baxter, J. Phys. C 6, L445 (1973).
[18]R. B. Potts, Proc. Camb. Philos. Soc. 48, 106 (1952).
[19]S. Alexander, Phys. Lett. A 54, 353 (1975).
[20]M. Schick, J. S. Walker, and M. Wortis, Phys. Lett. A 58, 479 (1976); Phys. Rev. B 16, 2205 (1977).
[21]T. Niemeijer and J. M. J. van Leeuwen, Phys. Rev. Lett. 31, 1411 (1973); Physica (Utr.) 71, 17 (1974); in *Phase Transitions and Critical Phenomena*, edited by C. Domb and M. S. Green (Academic, New York, 1977), Vol. 6; J. M. J. van Leeuwen, in *Fundamental Problems in Statistical Mechanics*, edited by E. G. D. Cohen (North-Holland, Amsterdam, 1975), Vol. 3.
[22]L. P. Kadanoff, Phys. Rev. Lett. 34, 1005 (1975); L. P. Kadanoff, A. Houghton, and M. C. Yalabık, J. Stat. Phys. 14, 171 (1976).
[23]K. G. Wilson, Phys. Rev. B 4, 3174 (1971); 4, 3184 (1971); K. G. Wilson and J. Kogut, Phys. Rep. C 12, 75 (1974); M. E. Fisher, Rev. Mod. Phys. 46, 597 (1974).
[24]A. N. Berker and M. Wortis, Phys. Rev. B 14, 4946 (1976).
[25]L. P. Kadanoff, in *Proceedings of the International School of Physics "Enrico Fermi," Course 51*, edited by M. S. Green (Academic, New York, 1971).
[26]R. J. Baxter and F. Y. Wu, Phys. Rev. Lett. 31, 1294 (1973); Aust. J. Phys. 27, 357 (1974); R. J. Baxter, M. F. Sykes, and M. G. Watts, J. Phys. A 8, 245 (1975).
[27]M. Wortis, Phys. Lett. A 47, 445 (1974).
[28]A. N. Berker, Phys. Rev. B 12, 2752 (1975).
[29]A. A. Migdal, Zh. Eksp. Teor. Fiz. 69, 1457 (1975) [Sov. Phys.-JETP 42, 743 (1976)].
[30]L. P. Kadanoff, Ann. Phys. (N.Y.) 100, 359 (1976).
[31]In previous, unpublished work, M. R. Giri and M. J. Stephen similarly recovered, using a Migdal transformation, the global, multicritical phase diagram obtained in Ref. 24 for the Blume-Emery-Griffiths-Potts model.
[32]Since the Blume-Emery-Griffiths model ($q=2$) and the model studied here ($q=3$) belong to one family of q-state Potts models with vacancies, it is not surprising that the global phase diagrams derived in Ref. 24 and here are topologically equivalent. However, certain phase boundaries must be "renamed" in completing the connection: The Ising critical surface, the Ising critical end-line, the ordinary tricritical line, and the Potts tricritical point in Ref. 24 are respectively "replaced" here by the Potts tricritical surface, the Potts tricritical end-line, the fourth-order line, and the four-state Potts transition point. The multiplicities of the coexisting ordered phases are, respectively, two and three.
[33]M. D. Chinn and S. C. Fain, Phys. Rev. Lett. 39, 146 (1977).
[34]If one were lattice modeling a two-dimensional gas on a uniform substrate, the relation between chemical potential μ and the interaction constant Δ of our Hamiltonian (2.2) would be $\Delta=-\mu/kT+\ln\lambda^2/v_0=-\mu/kT-\ln T/\tau$, where $\lambda=(2\pi\hbar^2/mkT)^{1/2}$ is the thermal wavelength of the adsorbate, and v_0 is the lattice-gas cell area. The second term arises from the translational kinetic energy of an ideal gas (Ref. 2). For krypton, τ is 0.695 °K, which, being much smaller than the experimental transition temperatures, justifies the neglect of quantum mechanical effects. However, krypton atoms absorbed onto graphite feel a nonuniform substrate potential. Thus, although the relation given above must be true at high temperatures in the fluid phases, we expect the second, kinetic term not to appear at low temperatures (and thereby the third law not to be violated), since all adatoms should be well localized at the potential minima (see Ref. 20 for another discussion). The uncertainty as to how this term is phased out does not affect our reported results, since we never use the connection to μ.
[35]For thermodynamic, also called annealed, impurities, the partition function is averaged over impurity configurations, as opposed to quenched inpurities for which the free energy is averaged.
[36]M. Blume, V. J. Emery, and R. B. Griffiths, Phys. Rev. A 4, 1071 (1971).
[37]Mean-field studies of the Blume-Emery-Griffiths model are Ref. 36; D. Mukamel and M. Blume, Phys. Rev. A 10, 610 (1974); J. Lajzerowicz and J. Sivardière, *ibid.* 11, 2079 (1975); J. Sivardière and J. Lajzerowicz, *ibid.* 11, 2090 (1975); 11, 2101 (1975); D. Furman, S. Dattagupta, and R. B. Griffiths, Phys. Rev. B 15, 441 (1977). Reference 24 is a renormalization-group study.
[38]M. J. Stephen, Phys. Lett. A 56, 149 (1976); C. Jayaprakash, J. Chalupa, and M. Wortis, Phys. Rev. B 15, 1495 (1977); S. Kirkpatrick, *ibid.* 15, 1533 (1977).
[39]J. V. José, L. P. Kadanoff, S. Kirkpatrick, and D. R. Nelson, Phys. Rev. B 16, 1217 (1977). A different treatment of the single-site interaction in the Migdal recursion was recently proposed by V. J. Emery and R. H. Swendsen, Phys. Lett. A 64, 325 (1977).
[40]D. R. Nelson and M. E. Fisher, Ann. Phys. (N.Y.) 91, 226 (1975).
[41]M. Nauenberg and B. Nienhuis, Phys. Rev. Lett. 33, 1598 (1974); B. Nienhuis and M. Nauenberg, Phys. Rev. B 11, 4153 (1975).
[42]Our assignment of the labels "in-registry solid," "liquid," and "gas" is based on sublattice ordering ($n_a \stackrel{?}{=} n_b$) and total density (n) considerations.
[43]In the mean-field approximation treatment of the PLG, the relative positions of the phases are qualitatively as in Fig. 6. However, much of the phase boundaries is different: The first-order surface between the solid and the gas continues, to become a first-order surface between the solid and the liquid; thus, there is no special line such as $B^{(0)}P_4$ in Fig. 6. The topological analog of $P_4P_{3E}^{(\infty)}$ is not a higher-order transition line, rather just a first-order line where the liquid-gas first-order surface meets the solid-fluid first-order surfaces. The analog of $P_4C^{(\infty)}$ is still a line of critical points, the only locus of higher-order transition. The analog of P_4 is a critical end-point, and occurs outside the four-state Potts subspace. The actual four-state Potts transition occurs as first-order at an otherwise undistinguished point on the $P_4P_{3E}^{(\infty)}$ analog. This picture violates pieces of exact information (Sec. II B), which can be associated with the failure of mean-field type approximations to yield the continuous three- and four-state Potts transitions (Refs. 15–17 and 24). The mean-field approximation for the PLG is also worse, compared to our renormalization-group approximation, with respect to the quantitative locations of the transitions.

[44]From our $K/J > 4$ phase-diagram cross sections, one could speculate on the possibility of studying bulk solid-fluid systems as q-state Potts lattice gases, with $q \to \infty$ in an appropriate continuum limit.
[45]M. Suzuki, Prog. Theor. Phys. 51, 1992 (1974); J. D. Gunton and T. Niemeijer, Phys. Rev. B 11, 567 (1975).
[46]I. G. Enting, J. Phys. A 7, 1617 (1974); 7, 2181 (1974).
[47]I. G. Enting, J. Phys. A 8, L35 (1975).
[48]T. W. Burkhardt, H. J. F. Knops, and M. den Nijs, J. Phys. A 9, L179 (1976).
[49]C. Dasgupta, Phys. Rev. B 15, 3460 (1977); S. E. Ashley and M. B. Green, J. Phys. A 9, L165 (1976).
[50]Other, nonvariational renormalization-group results are: $y_T(q=3) = 1.11$ in Ref. 24, 1.06 in M. Schick and R. B. Griffiths, J. Phys. C 10, 2123 (1977); $y_T(q=4) = 1.30$ in H. J. F. Knops, J. Phys. A 8, 1508 (1975).
[51]B. Nienhuis and M. Nauenberg, Phys. Rev. Lett. 35, 477 (1975).
[52]The separation of the branch $F_S B$ from $n = 1$ is a measure of how much imperfection the solid phase can accommodate, this causing the density to fall below the $n = 1$ of the perfect solid. One might reason that an experimental solid phase could accommodate more imperfections, because these could be stabilized around defects of the graphite substrate. The temperature-independence (vertical appearance) of $(F_S B)_{\text{expt}}$ gives credence to this argument that its position is dictated by quenched graphite defects rather than thermal fluctuations in the many-body system of adatoms.
[53](a) B. Mihura and D. P. Landau, Phys. Rev. Lett. 38, 977 (1977); (b) G. Stell, H. Narang, and C. K. Hall, Phys. Rev. Lett. 28, 292 (1972); C. K. Hall and G. Stell, Phys. Rev. A 7, 1679 (1973).
[54]Another theoretical derivation of this upward concavity is in F. A. Putnam (unpublished).
[55]T. de Neef and I. G. Enting, J. Phys. A 10, 801 (1977).
[56]F. J. Wegner, J. Phys. C 7, 2098 (1974).
[57]Reference 24 also showed that analogous quantities, such as $y_2(B^*)$, $y_2(P_4^*)$, and $y_2(C^*)$ here, have similar accuracies.
[58]For other realizations of the four-state Potts transition in adsorbed monolayers, see E. Domany, M. Schick, and J. S. Walker, Phys. Rev. Lett. 38, 1148 (1977).
[59]M. Schick (private communication).
[60]J. J. Lander and J. Morrison, Surf. Sci. 6, 1 (1967).
[61]M. N. Barber, J. Phys. A 9, L171 (1976).
[62]Reference 20 discusses the subdominant eigenvalue exponent of Baxter-Wu fixed points, including other renormalization-group results: D. Imbro and P. C. Hemmer, Phys. Lett. A 57, 297 (1976); M. P. N. den Nijs, A. M. M. Pruisken, and J. M. J. van Leeuwen, Physica (Utr.) A 84, 539 (1976).
[63]R. Wolfe and J. R. Sams, J. Phys. Chem. 69, 1129 (1965).
[64]J. O. Hirschfelder, C. F. Curtiss, and R. B. Bird, *Molecular Theory of Gases and Liquids* (Wiley, New York, 1964).
[65]H. Taub, K. Carneiro, J. K. Kjems, L. Passell, and J. P. McTague, Phys. Rev. B 16, 4551 (1977).
[66]We are grateful to A. Aharony for bringing to our attention these points.